A full-dimensional quantum dynamical study of H_2+H_2 collisions: Coupled-states versus close-coupling formulation

Alex Bohr,[1] Stephen Paolini,[1] Robert C. Forrey,[1,a)] N. Balakrishnan,[2] and P. C. Stancil[3]
[1]*Department of Physics, Pennsylvania State University, Berks Campus, Reading, Pennsylvania 19610-6009, USA*
[2]*Department of Chemistry, University of Nevada Las Vegas, Las Vegas, Nevada 89154, USA*
[3]*Department of Physics and Astronomy and the Center for Simulational Physics, University of Georgia, Athens, Georgia 30602, USA*

(Received 6 December 2013; accepted 25 January 2014; published online 11 February 2014)

Collision-induced energy transfer involving H_2 molecules plays an important role in many areas of physics. Kinetic models often require a complete set of state-to-state rate coefficients for H_2+H_2 collisions in order to interpret results from spectroscopic observations or to make quantitative predictions. Recent progress in full-dimensional quantum dynamics using the numerically exact close-coupling (CC) formulation has provided good agreement with existing experimental data for low-lying states of H_2 and increased the number of state-to-state cross sections that may be reliably determined over a broad range of energies. Nevertheless, there exist many possible initial states (e.g., states with high rotational excitation) that still remain elusive from a computational standpoint even at relatively low collision energies. In these cases, the coupled-states (CS) approximation offers an alternative full-dimensional formulation. We assess the accuracy of the CS approximation for H_2+H_2 collisions by comparison with benchmark results obtained using the CC formulation. The results are used to provide insight into the orientation effects of the various internal energy transfer mechanisms. A statistical CS approximation is also investigated and cross sections are reported for transitions which would otherwise be impractical to compute. [http://dx.doi.org/10.1063/1.4864357]

I. INTRODUCTION

Collision-induced energy transfer involving hydrogen molecules plays an important role in many areas of astrophysics since H_2 is the most abundant molecule in the interstellar medium[1] and is the dominant coolant in primordial and low-metallicity gas.[2] Hydrogen molecules are often used to determine the temperature and density structure of the gas and to provide diagnostics through emission, absorption, and fluorescence. The rovibrational level populations of the molecules can be very different from a thermal distribution when there is a significant amount of external energy input in the system. Examples include photodissociation regions, star-forming regions, circumstellar shells, and other molecular regions of low density. These environments often experience a significant departure from local thermodynamic equilibrium (LTE) due to shocks and UV radiation from a nearby star or star cluster.[3–5] In order to accurately model these environments, it is necessary to solve a master equation for the level populations. This requires detailed knowledge of the state-to-state rate coefficients for a variety of microphysical processes including H_2+H_2 collisions.

Experimental studies of H_2 molecules are difficult due to the lack of a permanent dipole moment, so measurements of H_2+H_2 collisional data have been sparse.[6–11] Consequently, theoretical calculations have been and continue to be the primary source of state-resolved rate coefficients for astrophysical modeling. Uncertainties in the theoretical calculations arise from three contributions: (i) accuracy of the adopted potential energy surface (PES), (ii) level of decoupling approximation used in the scattering formulation, and (iii) numerical convergence with respect to the basis set size. Early theoretical studies of H_2+H_2 collisions were performed by Green[12] using the numerically exact close-coupling (CC) formulation within the rigid rotor approximation, which assumes the vibrational motion of each molecule is frozen. Later studies provided a full-dimensional PES for the four atom system[13–16] which allowed the rigid rotor formulation to be extended to include vibrational motion.[17,18] More recently, a series of quantum dynamics calculations have been reported[19–24] which use a full-dimensional CC formulation to compute the collision cross sections. The results of these calculations were shown to provide good agreement with experimental data in the limited cases where experimental data are available. The calculations have also increased the number of state-to-state cross sections that may be reliably determined over a broad range of energies. Nevertheless, the CC calculations are extremely time-consuming and there exist many rovibrationally excited states which have cross sections that are impractical to compute using the CC formulation even at low collision energies. In these cases, a full-dimensional formulation may be used with a decoupling approximation to compute the cross sections. One of the most widely used decoupling approaches is the coupled-states (CS) approximation which has been formulated for diatom-diatom systems.[25,26] This approximation has been used to study vibrational relaxation and rotational

a)Electronic mail: rcf6@psu.edu

excitation in H_2+H_2 collisions[27–30] using the potential energy surfaces[13–15] that were available at the time. The more recent PES developed by Hinde[16] is believed to provide improved accuracy for the low-lying vibrational levels of H_2. The full-dimensional CC calculations[21,22] which used the Hinde PES showed the best agreement with the existing experimental data. For this reason, we have employed the Hinde PES for all calculations reported in this work and consider the CC results which use the Hinde PES to be the best benchmark for testing the accuracy of the CS approximation.

The CS formulation uses an effective orbital angular momentum $\bar{l}$ in the centrifugal potential which remains diagonal when the coupled equations are transformed from the space-fixed (SF) frame to the body-fixed (BF) frame. This approximation assumes that off-diagonal Coriolis couplings are negligible which reduces the number of coupled equations and allows them to be solved more efficiently. The error introduced by the neglected Coriolis couplings in the CS formulation has been studied numerically for the rigid rotor approximation[26,28,29] but as far as we are aware, there have been no comparable studies for the full-dimensional diatom-diatom case. Because the CS approximation represents a means to compute large amounts of data which may be used to model complex systems, it is important to provide error analysis of theoretical uncertainties. However, it would be impractical to perform such analysis for an entire set of state-to-state data. Therefore, in the present study, we have chosen a subset of possible transitions which should allow general trends in the error of the full-dimensional CS approximation to be understood. Comparison of CS and CC results are made for selected initial states at relatively low collision energies. Cross sections are then computed using the CS approach in its full implementation and in a reduced statistical approximation for an enlarged set of para-H_2+para-H_2 collisions over a wide range of energies. These cross sections, many of which would be computationally intractable to obtain using the CC method, should be useful for estimating state-to-state rate coefficients for temperatures up to several thousand K. In addition, the partial cross sections with respect to the BF projection of the internal angular momentum vector are used to gain mechanistic insights into the energy transfer process, including orientation effects.

II. THEORY

Here we review the quantum mechanical CC and CS formulations for diatom-diatom collisions.[12,25,26] The Hamiltonian of the four-atom system

$$H(\vec{r}_1, \vec{r}_2, \vec{R}) = T(\vec{r}_1) + T(\vec{r}_2) + T(\vec{R}) + V(\vec{r}_1, \vec{r}_2, \vec{R}), \quad (1)$$

is composed of a radial kinetic energy term $T(\vec{R})$ describing the center-of-mass motion, two kinetic energy terms $T(\vec{r}_1)$ and $T(\vec{r}_2)$ for each diatomic molecule, and the potential

$$V(\vec{r}_1, \vec{r}_2, \vec{R}) = U(\vec{r}_1, \vec{r}_2, \vec{R}) + V(\vec{r}_1) + V(\vec{r}_2), \quad (2)$$

where $V(\vec{r}_1)$ and $V(\vec{r}_2)$ are the two-body potential energies of the isolated H_2 molecules and $U(\vec{r}_1, \vec{r}_2, \vec{R})$ is the four-body potential which describes the interaction between the molecules which vanishes at large molecule-molecule separations. The angular dependence of the interaction potential may be expanded as

$$U(\vec{r}_1, \vec{r}_2, \vec{R}) = \sum_{\lambda} A_\lambda(r_1, r_2, R)\, Y_\lambda(\hat{r}_1, \hat{r}_2, \hat{R}) \quad (3)$$

with

$$Y_\lambda(\hat{r}_1, \hat{r}_2, \hat{R}) = \sum_{m_\lambda} \langle \lambda_1 m_{\lambda_1} \lambda_2 m_{\lambda_2} | \lambda_{12} m_{\lambda_{12}} \rangle\, Y_{\lambda_1 m_{\lambda_1}}(\hat{r}_1) \times Y_{\lambda_2 m_{\lambda_2}}(\hat{r}_2)\, Y^*_{\lambda_{12} m_{\lambda_{12}}}(\hat{R}), \quad (4)$$

where λ and m_λ represent the triple indices $\lambda \equiv \lambda_1\lambda_2\lambda_{12}$ and $m_\lambda \equiv m_{\lambda_1} m_{\lambda_2} m_{\lambda_{12}}$, respectively, $\langle ... | ... \rangle$ represents a Clebsch-Gordan coefficient, and $Y_{lm}(\hat{r})$ is a spherical harmonic. The total wave function for the four-atom system is expanded in terms of a diabatic basis set which contains the product function

$$\chi_{v j_1 j_2}(r_1, r_2) = \chi_{v_1 j_1}(r_1) \chi_{v_2 j_2}(r_2) \quad (5)$$

of H_2 wave functions $\chi_{v_i j_i}(r_i)$ with vibrational and rotational quantum numbers v_i and j_i, respectively. To compact the notation, we define $v \equiv v_1 v_2$ and $j \equiv j_1 j_2 j_{12}$ for the quantum numbers, and $[x] \equiv (2x + 1)$ for the degeneracy factors. The radial interaction potential, obtained by integrating over the internal bound coordinates, is given by

$$B^{\lambda}_{v j_1 j_2; v' j'_1 j'_2}(R) = \int_0^\infty \int_0^\infty \chi_{v j_1 j_2}(r_1, r_2) A_\lambda(r_1, r_2, R) \times \chi_{v' j'_1 j'_2}(r_1, r_2) r_1^2 r_2^2 dr_1 dr_2 \,. \quad (6)$$

The form of the full potential matrix depends on the CC and CS scattering formulations as discussed below. In both cases, a set of coupled equations must be solved in order to obtain the desired cross section. For indistinguishable molecules, the state-to-state cross section for collision energy E_c is given by a statistically weighted sum of the exchange-permutation symmetrized cross sections, $\sigma^{\varepsilon_P = \pm 1}$, as follows:

$$\sigma_{v_1 j_1 v_2 j_2 \to v'_1 j'_1 v'_2 j'_2}(E_c) = W^+ \sigma^{\varepsilon_P = +1} + W^- \sigma^{\varepsilon_P = -1}, \quad (7)$$

where $W^+ = 1$ and $W^- = 0$ for para-H_2 molecules (nuclear spin $I = 0$), and $W^+ = 2/3$ and $W^- = 1/3$ for ortho-H_2 molecules ($I = 1$). The exchange-permutation symmetry ε_P is given by $(-1)^{j_1+j_2+j_{12}+l}$ and $(-1)^{j_1+j_2+j_{12}+\bar{l}}$ for the CC and CS formulations, respectively.[25,26] For ortho-para collisions, there is no exchange symmetry present, and the full distinguishable basis set must be employed.

A. CC formulation

In the CC formulation, the total wave function is expanded as

$$\Psi(\vec{r}_1, \vec{r}_2, \vec{R}) = \frac{1}{R} \sum_{v,j,l,J,M} F^{JM}_{vjl}(R) \phi^{JM}_{vjl}(\vec{r}_1, \vec{r}_2, \hat{R}), \quad (8)$$

where l is the orbital angular momentum quantum number, J is the total angular momentum quantum number, and M is its

projection on a space-fixed axis. The diabatic functions

$$\phi_{vjl}^{JM}(\vec{r}_1, \vec{r}_2, \hat{R}) = \chi_{vj_1j_2}(r_1, r_2)\langle \hat{r}_1\hat{r}_2\hat{R}\,|\,jlJM\rangle, \tag{9}$$

serve as basis functions where $\langle \hat{r}_1\hat{r}_2\hat{R}\,|\,jlJM\rangle$ denote rotational wave functions in the total angular momentum representation. The radial functions $F_{vjl}^{JM}(R)$ are obtained by solving the set of coupled equations,

$$\left[-\frac{\hbar^2}{2\mu}\frac{d^2}{dR^2} + \frac{\hbar^2 l(l+1)}{2\mu R^2} - E_c\right] F_{vjl}^{J}(R) + \sum_{v'j'l'} V_{vjl;v'j'l'}^{J}(R)\, F_{v'j'l'}^{J}(R) = 0\,, \tag{10}$$

where μ is the reduced mass of the molecule-molecule system. The coupled-equations are independent of M, so it is dropped from the notation. The potential matrix elements are given in terms of 3j, 6j, and 9j symbols as

$$V_{vjl;v'j'l'}^{J}(R) = (4\pi)^{-3/2}\sum_{\lambda}(-1)^{j_1'+j_2'+j_{12}+J}\left([j_1][j_2][j_{12}][l][j_1'][j_2'][j_{12}'][l'][\lambda_1][\lambda_2][\lambda]^2\right)^{1/2} \times \begin{pmatrix} l' & \lambda & l \\ 0 & 0 & 0 \end{pmatrix}\begin{pmatrix} j_1' & \lambda_1 & j_1 \\ 0 & 0 & 0 \end{pmatrix}\begin{pmatrix} j_2' & \lambda_2 & j_2 \\ 0 & 0 & 0 \end{pmatrix}\begin{Bmatrix} l & l' & \lambda \\ j_{12}' & j_{12} & J \end{Bmatrix}\begin{Bmatrix} j_{12} & j_2 & j_1 \\ j_{12}' & j_2' & j_1' \\ \lambda & \lambda_2 & \lambda_1 \end{Bmatrix} B_{vj;v'j'}^{\lambda}(R). \tag{11}$$

The numerical solution to (10) is propagated to match the asymptotic boundary condition. The exchange permutation symmetrized cross sections are obtained from

$$\sigma^{\varepsilon_P} = \frac{\pi(1+\delta_{v_1v_2}\delta_{j_1j_2})(1+\delta_{v_1'v_2'}\delta_{j_1'j_2'})}{(2j_1+1)(2j_2+1)2\mu E_c} \times \sum_{Jj_{12}j_{12}'ll'\varepsilon_I}(2J+1)\left|T_{vjl;v'j'l'}^{J\varepsilon_I\varepsilon_P}(E_c)\right|^2, \tag{12}$$

where T is the transition matrix and $\varepsilon_I = (-1)^{j_1+j_2+l}$ is the eigenvalue of the spatial inversion operator.

B. CS formulation

In the CS formulation, the total wave function is expanded as

$$\Psi(\vec{r}_1, \vec{r}_2, \vec{R}) = \frac{1}{R}\sum_{v,j,J,M,\Omega} F_{vj\Omega}^{JM}(R)\phi_{vj\Omega}^{JM}(\vec{r}_1, \vec{r}_2, \hat{R}), \tag{13}$$

where the coordinates now refer to a BF axis and the quantum number Ω refers to the BF projection of j_{12}. The diabatic basis functions are given by

$$\phi_{vj\Omega}^{JM}(\vec{r}_1, \vec{r}_2, \hat{R}) = \chi_{vj_1j_2}(r_1, r_2)\langle \hat{r}_1\hat{r}_2\hat{R}\,|\,j\Omega JM\rangle, \tag{14}$$

where $\vec{l} = \vec{J} - \vec{j}_{12}$ defines the centrifugal operator $\hat{l}^2$ which operates on the rotational wave function $\langle \hat{r}_1\hat{r}_2\hat{R}|\,j\Omega JM\rangle$ in the BF frame. The potential matrix elements[25,26]

$$V_{vj;v'j'}^{\Omega}(R) = (4\pi)^{-3/2}\sum_{\lambda}(-1)^{j_1'+j_2'+j_{12}'+\Omega}\left([j_1][j_2][j_{12}][j_1'][j_2'][j_{12}'][\lambda_1][\lambda_2][\lambda]^2\right)^{1/2} \times \begin{pmatrix} j_1' & \lambda_1 & j_1 \\ 0 & 0 & 0 \end{pmatrix}\begin{pmatrix} j_2' & \lambda_2 & j_2 \\ 0 & 0 & 0 \end{pmatrix}\begin{pmatrix} j_{12}' & \lambda & j_{12} \\ \Omega & 0 & -\Omega \end{pmatrix}\begin{Bmatrix} j_{12} & j_2 & j_1 \\ j_{12}' & j_2' & j_1' \\ \lambda & \lambda_2 & \lambda_1 \end{Bmatrix} B_{vj;v'j'}^{\lambda}(R) \tag{15}$$

are diagonal with respect to Ω and are independent of J. The CS approximation is made by assuming that the off-diagonal elements of $\hat{l}^2$ with respect to Ω are small and that the diagonal elements may be approximated by $\hbar^2\bar{l}(\bar{l}+1)$ where the effective orbital angular momentum quantum number $\bar{l}$ replaces J. The radial functions $F_{vj\Omega}^{JM}(R)$ in Eq. (13) are then written as $F_{vj}^{\Omega}(R)$ and obtained by solving the set of coupled equations,

$$\left[-\frac{\hbar^2}{2\mu}\frac{d^2}{dR^2} + \frac{\hbar^2\bar{l}(\bar{l}+1)}{2\mu R^2} - E_c\right] F_{vj}^{\Omega}(R) + \sum_{v'j'} V_{vj;v'j'}^{\Omega}(R)\, F_{v'j'}^{\Omega}(R) = 0. \tag{16}$$

This set of Eq. (16) is considerably more compact than the set of Eq. (10) due to the decoupling of the orbital angular momentum. The exchange permutation symmetrized cross sections are given by

$$\sigma^{\varepsilon_P} = \frac{\pi(1+\delta_{v_1v_2}\delta_{j_1j_2})(1+\delta_{v_1'v_2'}\delta_{j_1'j_2'})}{(2j_1+1)(2j_2+1)2\mu E_c} \times \sum_{j_{12}j_{12}'\bar{l}\Omega} (2\bar{l}+1)\left|T^{\bar{l}\Omega\varepsilon_P}_{vj;v'j'}(E_c)\right|^2. \quad (17)$$

Here, the inversion symmetry is ignored since the symmetrized potential matrix elements are identical to the unsymmetrized elements except when $\Omega = 0$.[25,26] The sum over Ω assumes positive and negative values such that $|\Omega| \leq \Omega_{max} = j_1 + j_2$. In practice, only non-negative values of Ω are computed and the positive Ω contributions are doubled.

A statistical approximation was introduced[26] which further assumes that all of the contributions from individual values of Ω are identical. This assumption yields the cross section

$$\sigma^{\varepsilon_P} = \frac{\pi(1+\delta_{v_1v_2}\delta_{j_1j_2})(1+\delta_{v_1'v_2'}\delta_{j_1'j_2'})}{(2j_1+1)(2j_2+1)2\mu E_c} \times \sum_{j_{12}j_{12}'\bar{l}} (2\bar{l}+1)\left[2\min\left(j_{12}, j_{12}'\right)+1\right]\left|T^{\bar{l}\bar{\Omega}\varepsilon_P}_{vj;v'j'}(E_c)\right|^2, \quad (18)$$

where $\bar{\Omega}$ is the single value used in the calculation. The statistical CS approximation is tested for the case $\bar{\Omega} = 0$ in Sec. III C.

III. RESULTS

The results shown in this work are for para-H_2+para-H_2 collisions. The calculations were performed using a modified version of the TwoBC code.[31] The log-derivative matrix propagation method of Johnson[32] and Manolopoulos[33] was used to integrate the coupled equations from $R = 3 - 53$ a.u. in steps of 0.05 a.u. All basis sets included $j_{max} = 10$ for $v = 0$, $j_{max} = 8$ for $v = 1$, and $j_{max} = 6$ for $v = 2$. Following previous work,[21,22,24] an energy cut-off was used to increase the computational efficiency. We found it convenient and sufficient to set the cut-off energy to 5000 cm^{-1} above the internal energy of the initial combined molecular state (CMS). Figure 1 shows the number of coupled channels that are required by the CC formulation for each value of J. The curves are labeled according to the notation $v_1 j_1 v_2 j_2$ for the initial CMS. The total number of combined molecular basis states is also included in the legend. The computational cost of the CC calculations increases rapidly with J and the number of CMSs. For $J = 10$, there are more than 3000 coupled equations for the 1008 and 1010 initial states. The number of coupled equations required by the CS formulation also increases with the number of CMSs but not with J (or equivalently $\bar{l}$) and is typically less than 500 as shown by the $J = 0$ points in Figure 1. The computational cost of the CS calculations is therefore manageable at high collision energies where large values of orbital angular momentum are required.

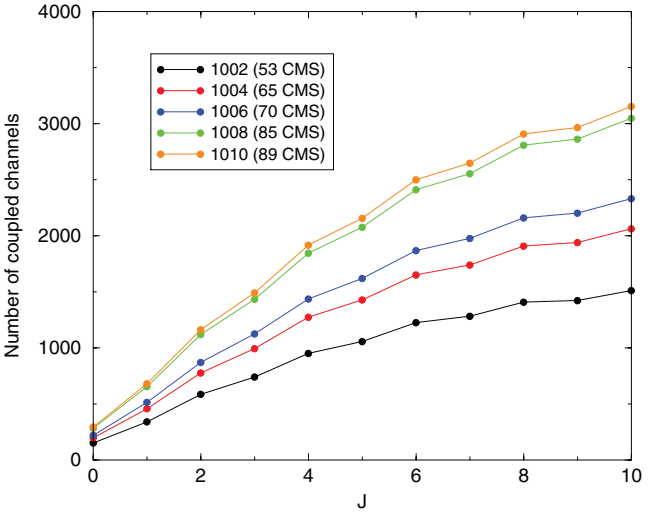

FIG. 1. Number of coupled channels as a function of total angular momentum J for the CC formulation. The curves are labeled according to the notation $v_1 j_1 v_2 j_2$ for the initial CMS. An energy cut-off of 5000 cm^{-1} above the internal energy of the initial CMS is assumed in determining the number of combined molecular basis states (see legend).

The CS calculations were carried out at ten equally spaced collision energies in each of the three decades: 10–100 K, 100–1000 K, and 1000–10 000 K using a maximum effective orbital angular momentum given by

$$\bar{l}_{max} = \begin{cases} 10, & E_c = 10\text{–}100\,\text{K} \\ 50, & E_c = 100\text{–}1000\,\text{K} \\ 100, & E_c = 1000\text{–}10\,000\,\text{K} \end{cases}. \quad (19)$$

Excellent agreement was seen at the E_c boundaries, and extensive convergence tests verified that the results were converged to within 5% or better with respect to the basis set. The CC calculations were performed for $E_c \leq 100$ K using $J_{max} = 10$, and excellent agreement with previous calculations[21]

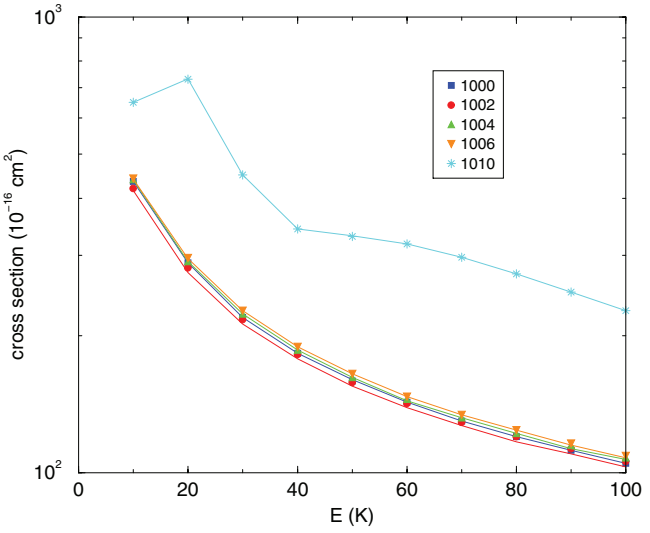

FIG. 2. Elastic cross sections for $H_2(v_1, j_1) + H_2(v_2, j_2)$ collisions. The curves are labeled according to the notation $v_1 j_1 v_2 j_2$ for the combined molecular state. The agreement between CC (points) and CS (lines) is excellent for each of these states.

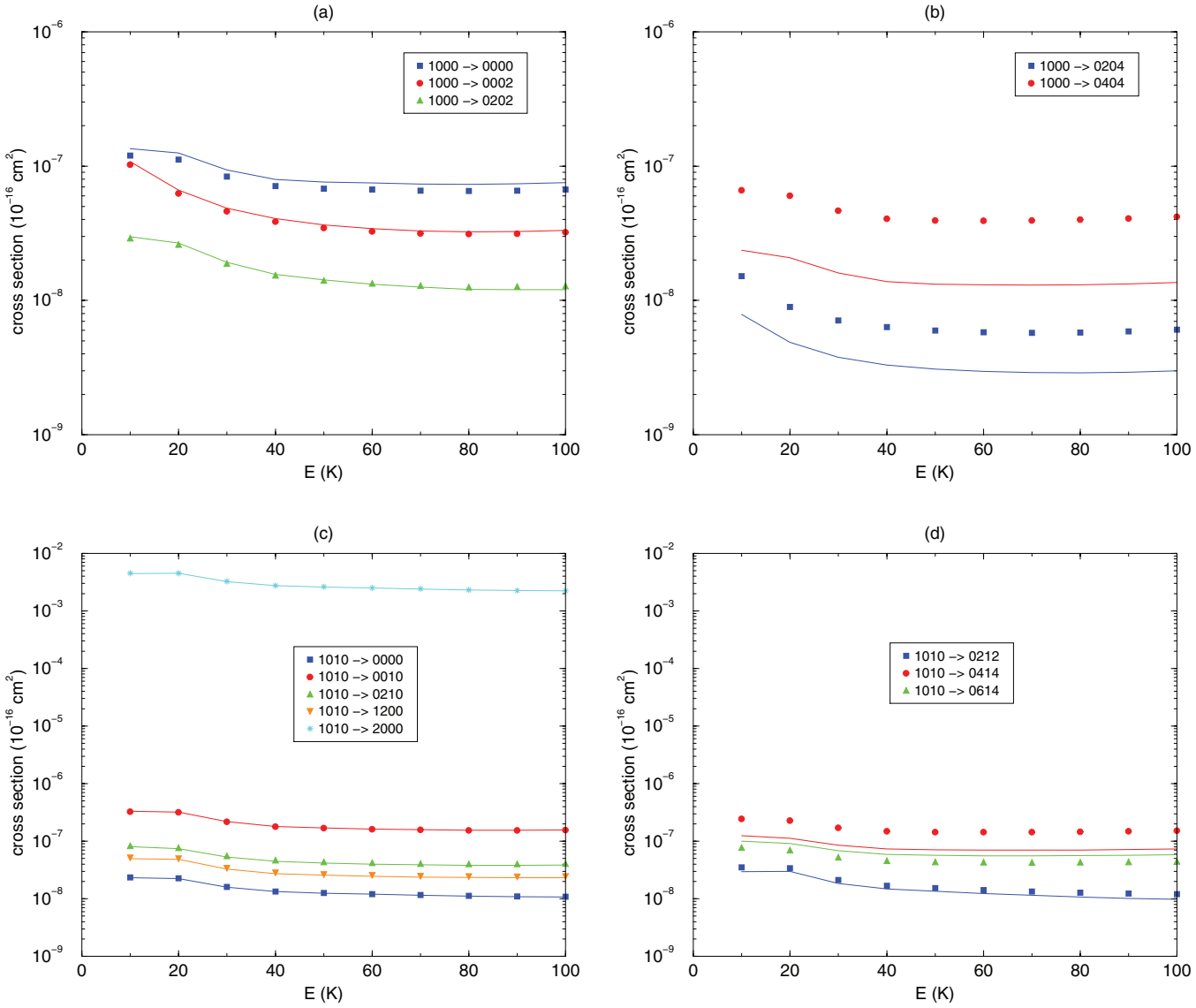

FIG. 3. Inelastic cross sections for 1000 and 1010 initial states using CC (points) and CS (lines) methods. Panels (a) and (c) show that the agreement is excellent for pure vibrational transitions and rotational transitions involving only one molecule. Panels (b) and (d) show that the agreement is not as good when both molecules undergo a multi-quantum rotational change. The discrepancies shown in (d) are less important than in (b) due to the QR transitions to the 2000 state shown in (c).

was observed. Additional CC results were obtained at these relatively low collision energies, and a comparison of the CC and CS methods was made to estimate the typical discrepancies that may be expected from the CS approximation.

A. Comparison of CS versus CC results

To assess the reliability of the CS calculations, we first benchmark select CS results against numerically exact CC results. Figure 2 compares the elastic scattering cross sections. The CC and CS calculations are shown as points and lines, respectively. The results are virtually identical for each state shown. The excellent agreement is not surprising for states 1000 and 1010 which have no rotational excitation because the diagonal matrix elements are identical for the two formulations when $j_{12} = 0$. The excellent agreement for the states 1002, 1004, and 1006 is encouraging considering that these states have internal rotational angular momentum, and it is states with high rotational excitation that become intractable in the CC formulation. It is noteworthy that the CS cross sections for the rotationally excited states converge more quickly with J than do the CC cross sections. This provides an additional computational cost savings for the CS calculations.

The CS and CC inelastic cross sections for 1000 and 1010 shown in Figure 3 are also in good agreement for pure vibrational transitions and rotational transitions involving only one molecule. These transitions tend to be among the most efficient for a given initial state, so the good agreement between the CS and CC results is encouraging. Figure 3 also shows inelastic cross sections for 1000 and 1010 which

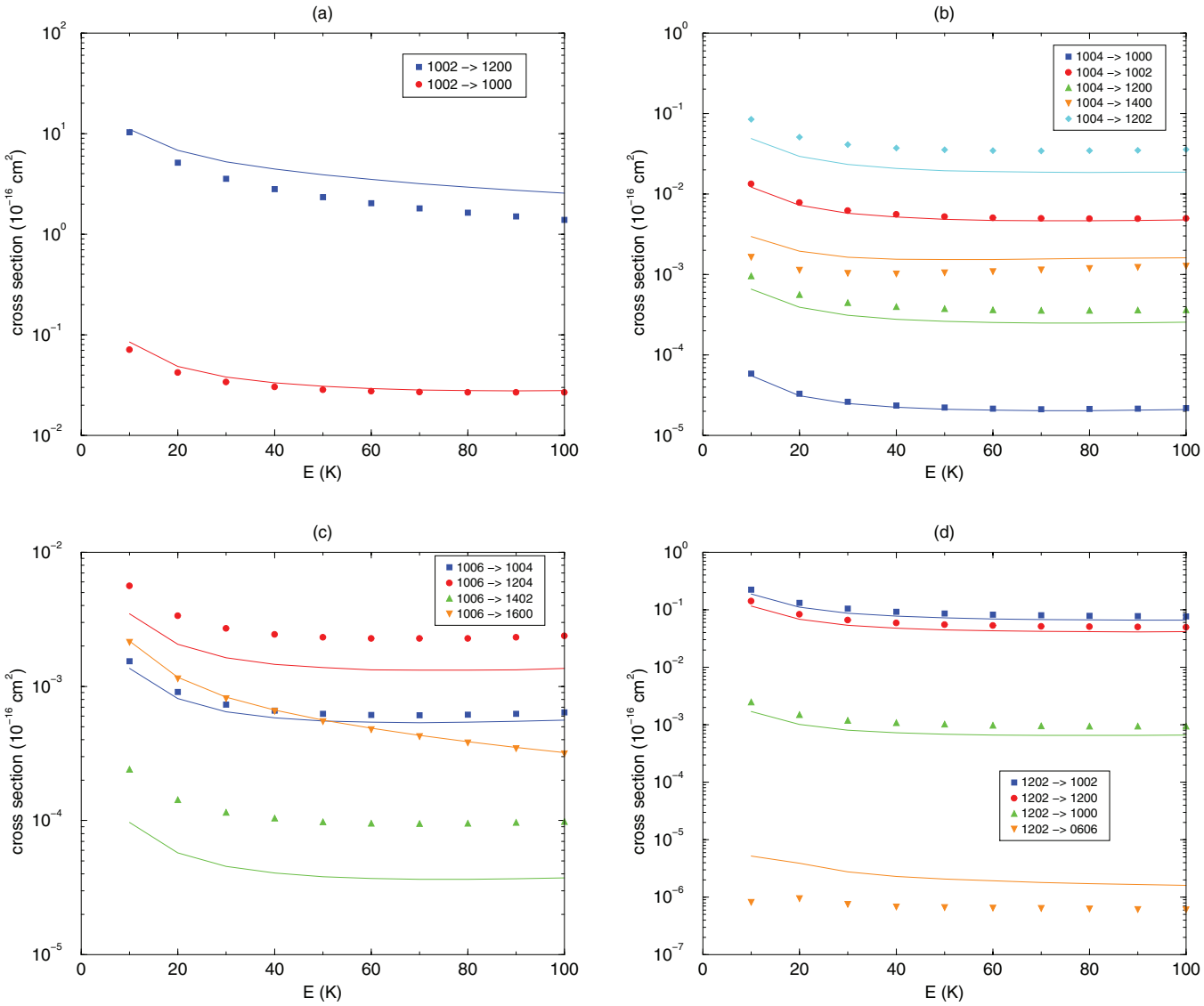

FIG. 4. CC versus CS inelastic cross sections for (a) 1002, (b) 1004, (c) 1006, and (d) 1202 initial states. The CS approximation is able to get the correct pattern of relative efficiencies, however, the discrepancy for some of the most important transitions may be as large as ∼50%. The accuracy of the CS approximation may improve when both molecules have rotational excitation [e.g., the 1202 initial state shown in panel (d)].

involve transitions where both molecules undergo a rotational change. In these cases, the agreement between the two scattering formulations is less satisfactory, especially when the transition involves a multi-quantum change in j. Fortunately, transitions which involve multi-quantum changes tend to be less efficient than transitions which involve only single-quantum changes, so the discrepancy introduced by the CS approximation may be reduced in significance for these cases. Nevertheless, there are examples which do not follow this trend. Figure 3(b) shows such a case for the 1000 initial state. The 1000 → 0404 cross section, which the CC calculation shows is the second largest at energies greater than 10 K, is about a factor of two smaller when calculated using the CS approximation. This discrepancy would incorrectly lower the cross section for this transition below that of the 1000 → 0002 transition (compare Figure 3(a)). Likewise, the 1010 → 0414 cross section is about two times smaller than it should be when calculated using the CS approximation (see Figure 3(d)). However, in this case, the quasi-resonant (QR) 1010 → 2000 transition is so dominant (see Figure 3(c)) that discrepancies contained in all other transitions are likely to be unimportant.

There are discrepancies in the CS results for initial states which are rotationally excited. Figure 4 shows several examples including the 1002, 1004, and 1006 initial states which showed virtually no error in the elastic scattering cross sections (see Figure 2). Differences between the CC and CS cross sections can be as large as ∼50%. Nevertheless, the CS approximation is able to predict the correct pattern of relative efficiencies and reproduce the correct energy dependence for these initial states. Therefore, it may be useful to employ a single low-energy CC calculation to "anchor" higher energy CS cross sections. This technique was found to work well for He+CO collisions.[34] Figure 4(d) shows

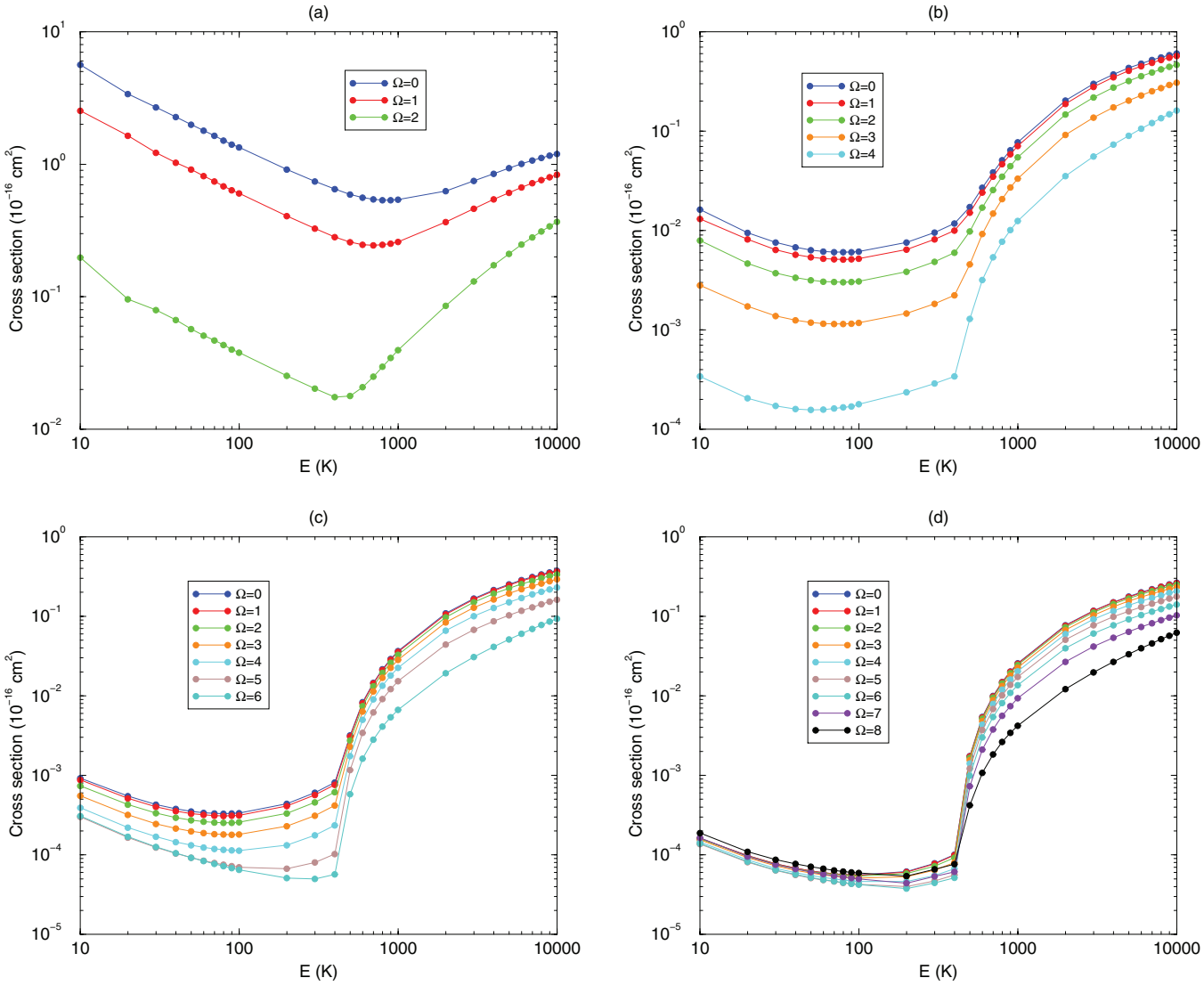

FIG. 5. Total CS quenching cross sections for (a) 1002, (b) 1004, (c) 1006, and (d) 1008 initial states. The upturns in the cross sections are due to the opening of the $v = 1, j = 2$ state (with the other molecule unchanged) which occurs at 484 K.

that the accuracy of the CS approximation for the dominant transitions can improve when both molecules have rotational excitation. For the 1202 initial state shown in the figure, the single molecule rotational de-excitation transitions are the most efficient and the agreement between the CS and CC results is excellent.

B. Dependence of CS cross sections on E_c and Ω

The statistical CS approximation introduced in Ref. 26 assumes that all of the individual Ω contributions are identical, so that the sum over Ω may be replaced by a single value of Ω with a statistical weight equal to $2\min(j_{12}, j'_{12}) + 1$ as shown in Eq. (18). In order to assess this approximation, it is helpful to study the variability in the partial cross sections for the different values of Ω. Figures 5–9 show a sample of our results for different initial states. In each figure, all Ω-contributions which connect to the initial state of interest are shown. The partial cross sections generally decrease with Ω due to the decreasing number of j_{12} values which can contribute to the transition. However, the pattern of this decrease is not always smooth and regular. For example, Figure 5(a) shows that the $\Omega = 2$ contribution to the quenching of the 1002 state is about a factor of 10 smaller than the $\Omega \leq 1$ contributions when the collision energy is less than 700 K. In this case, there is a QR transition to 1200 which is dominant at low energies (see Figure 4(a)) and only a single j_{12} value contributes to the transition for each partial cross section. The relative inefficiency of the $\Omega = 2$ contribution suggests that the QR mechanism is less likely to occur when the plane of the diatomic rotational motion is perpendicular to the BF z-axis. As the collision energy increases, additional states become available and the QR mechanism becomes less effective. The upturn in Figure 5(a) is due to the opening of the 1202 state for collision energies above 484 K. Similar upturns are found in the quenching cross sections for the 1004, 1006, and 1008 initial states shown in

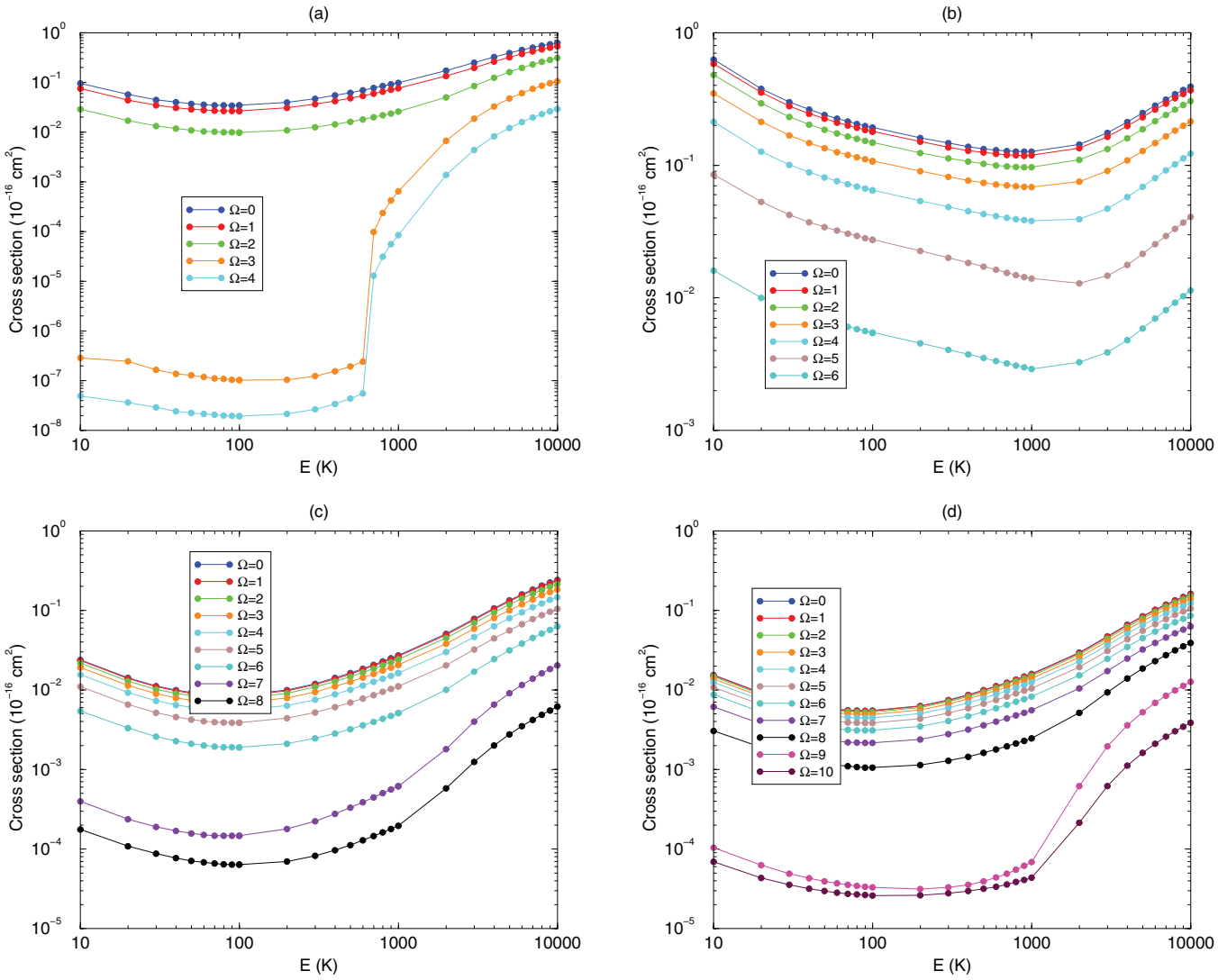

FIG. 6. Total CS quenching cross sections for (a) 1202, (b) 1204, (c) 1206, and (d) 1208 initial states. The step-like structure for $\Omega = 3$ and 4 in (a) is due to the opening of the 1400 and 1004 states above 603 K and 687 K, respectively. The more gradual upturns in (b)-(d) are due to the opening of the $v = 1, j = 4$ state (with the other molecule unchanged) which occurs at 1113 K.

Figure 5 due to the opening of the 1204, 1206, 1208 states, respectively. A general pattern may be observed in Figure 5 for initial states which have one molecule in the rotational ground state: as the rotational level of the other molecule increases, the contributions from all Ω tend to nearly converge, particularly at low collision energies, in accordance with the assumption used to justify the statistical approximation introduced previously.[26]

Figure 6 shows results for initial states that have rotational excitation in both molecules. Here, the decreasing contributions for large Ω are even more dramatic. This is due to the dominance of transitions to final states which have a maximum value of Ω which is less than the maximum initial value. For example, Figure 6(a) shows results for 1202 initial state whose quenching is dominated by transitions to 1002 and 1200 at low collision energies (see Figure 4(d)). At high energies, the 1004 and 1400 states become available, and the $\Omega = 3$ and $\Omega = 4$ contributions are substantially increased. In Figure 6(b), the low energy cross section is dominated by a QR transition to the 1402 state. Similar to the 1002 → 1200 transition described above, the QR mechanism is less effective when the planes of diatomic rotational motion are perpendicular to the BF z-axis. However, for the 1204 → 1402 transition, the strong decrease with Ω is also due to the decreasing number of j_{12} values that can have the larger projections. The upturn in Figure 6(b) is due to the opening of the 1404 state which combines with several other states to reduce the QR mechanism. The cross sections for the 1206 and 1208 initial states shown in Figures 6(c) and 6(d) are dominated at low energies by pure rotational transitions to 1006 and 1008, respectively. In both of these cases, the dominant final state has a maximum Ω which is two less than the maximum Ω allowed by the initial state, and consequently, the last two Ω-contributions to the total quenching cross section are significantly suppressed. As in Figure 6(a), the opening of additional final states with energy (primarily 1406 for Figure 6(c) and 1408 for Figure 6(d)) helps to close the gap between the Ω-contributions.

Figure 7(a) shows a case where there is significant structure in the energy dependence of the cross sections. For

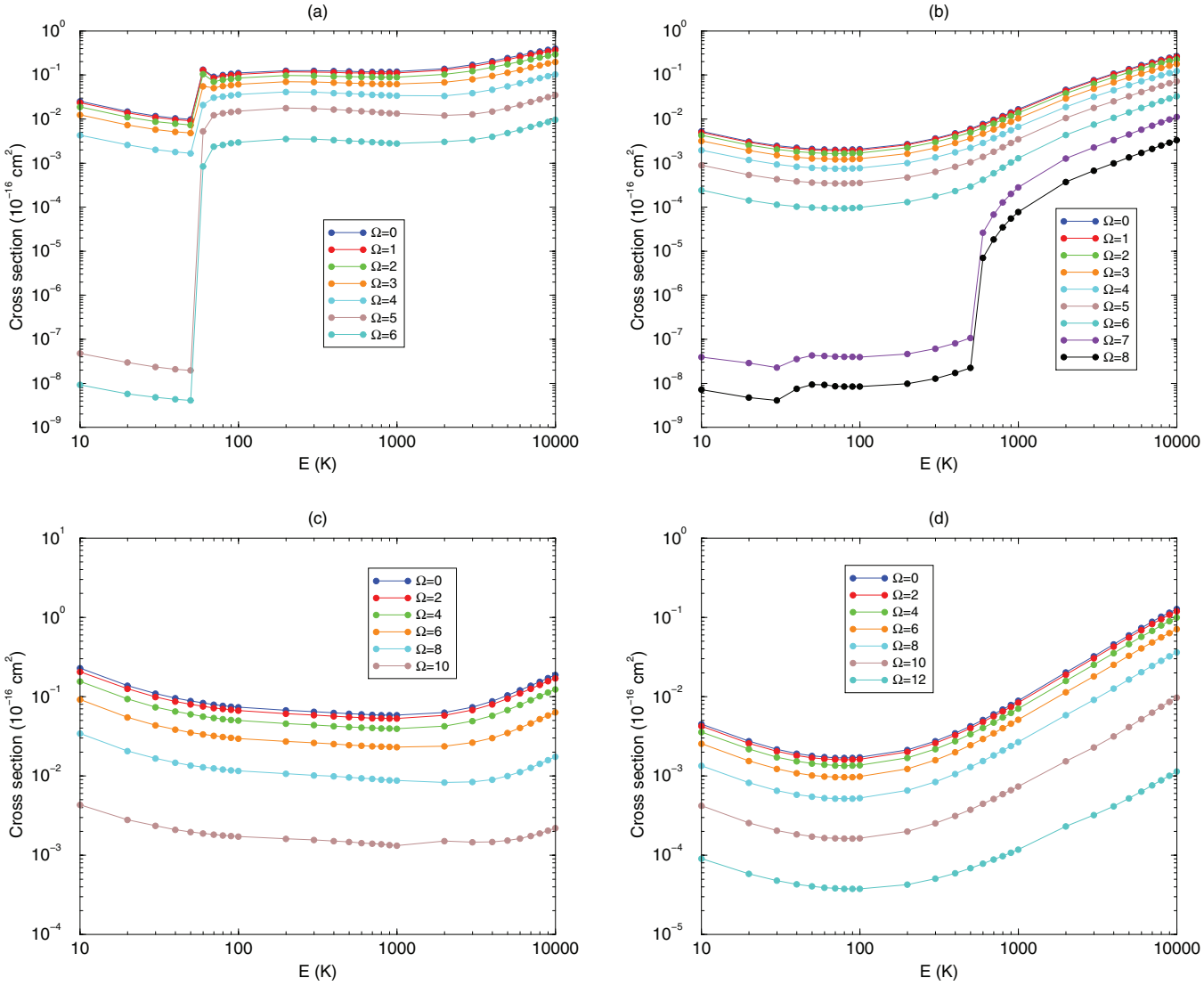

FIG. 7. Total CS quenching cross sections for (a) 1402, (b) 1404, (c) 1406, and (d) 1408 initial states. The step-like structure in (a) is due to the opening of the 1204 state above 59 K. In (b), the 1602 state opens at energies above 531 K and produces a step-like structure for the $\Omega = 7$ and 8 contributions.

collision energies at or below 50 K, the dominant transition is $1402 \rightarrow 1400$. Because $\Omega = 5$ and $\Omega = 6$ do not contribute to this transition, the curves are lower than the $\Omega < 5$ contributions by several orders of magnitude. At collision energies above 50 K, however, the 1204 final state becomes energetically allowed, and the $\Omega = 5$ and $\Omega = 6$ contributions become more significant. The total quenching cross section shows a step-like structure at the transition energy, 59 K, where the state 1204 first becomes energetically open. Such step-like structures in the total inelastic cross section are often observed at boundaries where QR transitions are available.[35] The quenching cross section shown in Figure 7(b) is dominated at low energies by pure rotational transitions to 1204 and 1402 final states. Consequently, the $\Omega = 7$ and $\Omega = 8$ contributions are negligible. At energies above 531 K, the 1602 state is open which produces a step-like increase for these last two Ω-contributions and a gradual increase for the other partial cross sections. The behavior for the quenching cross sections shown in Figures 7(c) and 7(d) is smooth and regular compared to the sharp structures described above. For the initial 1406 state, a QR transition to the 1604 state is dominant at low energies. The efficiency of the QR mechanism is again reduced when the rotational axes of the rotors are aligned with the BF z-axis, but the effect is masked by the large number of j_{12} values that can contribute to the QR transition. For energies greater than 1000 K, several other transitions have comparable efficiencies to that of the 1604 state, and a slight upturn in the cross section is seen. The 1408 initial state does not make a QR transition but instead allows competing transitions to take place with the 1606 and 1208 states being the most probable.

The 1602 initial state also allows many competing transitions, so the total quenching cross sections in Figure 8(a) resemble those in Figure 7(d). A step-like structure is observed for all partial cross sections shown in Figure 8(b) for the initial 1604 state at 100 K. Below this collision energy, the dominant

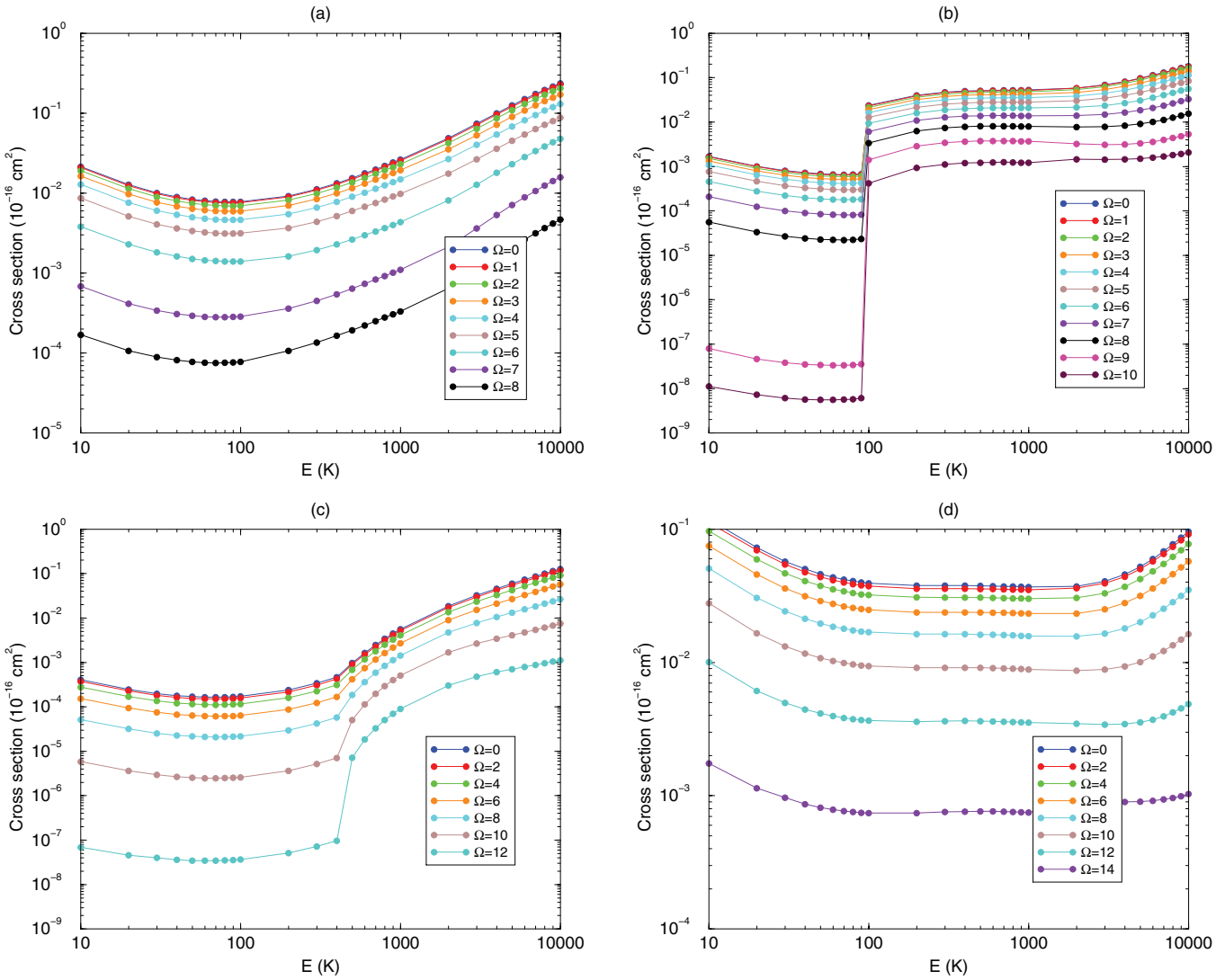

FIG. 8. Total CS quenching cross sections for (a) 1602, (b) 1604, (c) 1606, and (d) 1608 initial states. The step-like structure in (b) is due to the opening of the 1406 state above 91 K. The more gradual upturn in (c) is due to the opening of the 1804 and 1408 states above 442 K and 653 K, respectively.

transition is to the 1602 state which has no contribution from $\Omega = 9$ and $\Omega = 10$. At 100 K, a QR transition to the 1406 final state is accessible and all of the Ω contributions are enhanced including the $\Omega = 9$ and $\Omega = 10$ contributions which experience the largest increase. A more gradual step structure is seen in Figure 8(c) for the initial 1606 state. In this case, the low energy side of the step is dominated by transitions to 1604, 1406, and 0808 states. At high energies, relatively efficient transitions to the 1804 and 1408 states are allowed which adds to the other transitions and produces the step structure. For the 1608 initial state shown in Figure 8(d), the quenching is dominated by a QR transition to 1806 for all energies below 1000 K. Above this energy, several other transitions begin to contribute and an upturn is seen in the total quenching cross section.

Figure 9 shows results for initial states that have vibrational excitation in both molecules. The results are similar to those of initial states with the same rotational excitation in each molecule but with only a single vibrationally excited level. A notable difference, however, is the increased dominance of the $\Omega = 0$ contribution for the doubly vibrationally excited states compared to the singly excited states. Comparison of Figure 9(a) with Figure 6(a) shows that the falloff of the $\Omega = 3$ and $\Omega = 4$ contributions to the $j_1 = j_2 = 2$ cross section is far less when both molecules are vibrationally excited. Likewise, a comparison of Figure 9(b) with Figure 7(b) shows a significantly reduced falloff of the $\Omega = 7$ and $\Omega = 8$ contributions to the $j_1 = j_2 = 4$ cross section when both molecules are vibrationally excited. Figure 9(c) shows that the partial cross sections for initial state 1616 vary over only an order of magnitude for low energies, whereas those of 1606 (see Figure 8(c)) vary over several orders of magnitude. Figure 9 also shows that the cross sections decrease by roughly an order of magnitude with each increase in rotational excitation. This is due to the increasing energy gap which occurs for pure rotational transitions which are the dominant transitions for these molecular states.

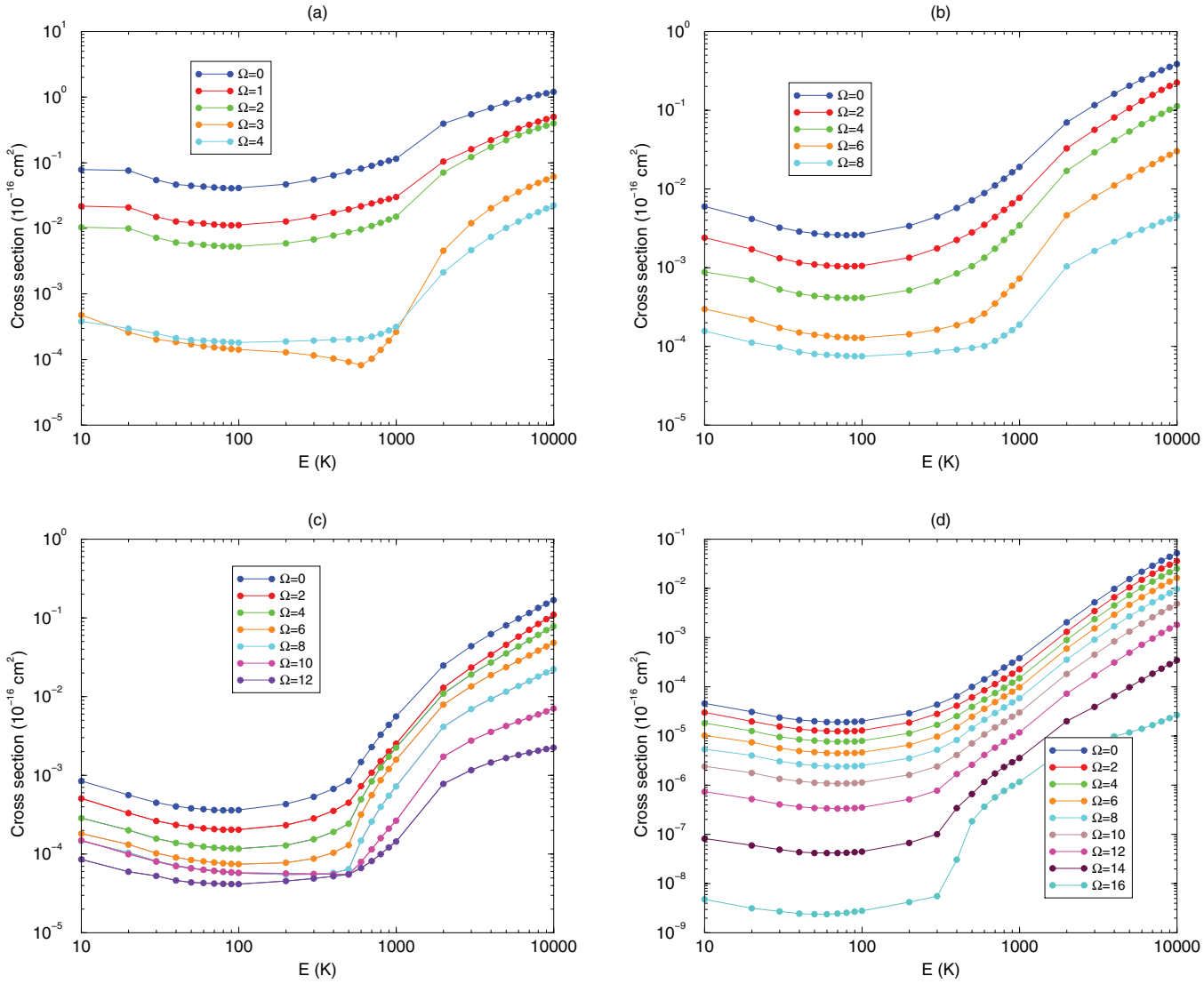

FIG. 9. Total CS quenching cross sections for (a) 1212, (b) 1414, (c) 1616, and (d) 1818 initial states. The cross sections for collisions between identical molecular states appear to decrease by about an order of magnitude with each increase in rotational excitation.

C. Comparison of the full and statistical CS approaches

The above observations suggest that the conventional statistical CS approximation would produce less than satisfactory results for H_2+H_2 collisions when the full set of partial cross sections is replaced by a single Ω-contribution multiplied by a statistical degeneracy factor. This was tested using the $\Omega = 0$ contribution, so we refer to this version as the "CS0" approximation. Tables I–IV show numerical results for the CS0 approximation along with those for a modified statistical approximation. In the modified version, only even non-negative Ω contributions are computed, and the positive Ω contributions are multiplied by a weight factor of 4 to account for the degeneracy of positive and negative projections and the neglect of odd-Ω contributions. This scheme is similar to a commonly used statistical approximation for the sum over J at high energies. In the present case, the computational effort is cut in half compared to the full CS approximation. Therefore, we refer to this version as the "half CS" approximation. Both statistical approximations are compared against the full CS results for the 1002, 1004, 1006, and 1008 initial states. The tables show that the half CS results are considerably more accurate than the CS0 results for most transitions. The accuracy for the largest cross sections improves as Ω_{max}, the maximum value of j_{12} for the initial state, increases. Generally, the largest discrepancies occur for transitions where $\min[\Omega_{max}, \Omega'_{max}] = 2$ which give typical differences of about 40% for the half CS approximation. This is due to the importance of the neglected $\Omega = 1$ contribution compared to the $\Omega = 0$ and $\Omega = 2$ contributions. As the number of contributing projections increases, the half CS statistical approximation generally improves. For transitions where $\min[\Omega_{max}, \Omega'_{max}] \geq 4$, the half CS approximation gives agreement to within 20% or better. The results of the CS0 approximation are more erratic and show differences exceeding 100% for many of the transitions. Because the full CS cross sections appear to depend on Ω in a relatively smooth fashion at high energies (see Figures 5–9), it is conceivable that the half CS approximation could be further improved

TABLE I. Comparison of full CS and statistical CS approximations for the 1002 initial state. Cross sections (Å^2) are shown at E = 100 K for the most efficient transitions in descending order. The left and right % difference columns compare the respective half CS and CS0 results with the full CS approximation. The smaller error is bold-faced in order to show that the half CS approximation performs better than the CS0 approximation in most cases.

Final state	Full CS	Half CS	CS0	% Difference	% Difference
1002	$0.103 \times 10^{+3}$	$0.101 \times 10^{+3}$	$0.105 \times 10^{+3}$	$0.200 \times 10^{+1}$	**$0.119 \times 10^{+1}$**
1200	$0.256 \times 10^{+1}$	$0.144 \times 10^{+1}$	$0.645 \times 10^{+1}$	**$0.437 \times 10^{+2}$**	$0.152 \times 10^{+3}$
1000	0.279×10^{-1}	0.279×10^{-1}	0.279×10^{-1}	0.000×10^{0}	0.000×10^{0}
0406	0.727×10^{-7}	0.642×10^{-7}	0.680×10^{-7}	$0.117 \times 10^{+2}$	**$0.655 \times 10^{+1}$**
0202	0.620×10^{-7}	0.555×10^{-7}	0.253×10^{-7}	**$0.105 \times 10^{+2}$**	$0.592 \times 10^{+2}$
0002	0.529×10^{-7}	0.500×10^{-7}	0.544×10^{-7}	$0.552 \times 10^{+1}$	**$0.291 \times 10^{+1}$**
0404	0.457×10^{-7}	0.261×10^{-7}	0.152×10^{-7}	**$0.430 \times 10^{+2}$**	$0.668 \times 10^{+2}$
0204	0.265×10^{-7}	0.156×10^{-7}	0.156×10^{-7}	$0.411 \times 10^{+2}$	$0.414 \times 10^{+2}$
0004	0.524×10^{-8}	0.416×10^{-8}	0.767×10^{-8}	**$0.207 \times 10^{+2}$**	$0.462 \times 10^{+2}$
0206	0.364×10^{-8}	0.388×10^{-8}	0.193×10^{-8}	**$0.656 \times 10^{+1}$**	$0.471 \times 10^{+2}$
0000	0.282×10^{-8}	0.282×10^{-8}	0.282×10^{-8}	0.000×10^{0}	0.000×10^{0}

TABLE II. Comparison of full CS and statistical CS approximations for the 1004 initial state. Cross sections (Å^2) are shown at E = 100 K for the most efficient transitions in descending order. The left and right % difference columns compare the respective half CS and CS0 results with the full CS approximation. The smaller error is bold-faced in order to show that the half CS approximation performs better than the CS0 approximation in most cases.

Final state	Full CS	Half CS	CS0	% Difference	% Difference
1004	$0.107 \times 10^{+3}$	$0.105 \times 10^{+3}$	$0.111 \times 10^{+3}$	**$0.144 \times 10^{+1}$**	$0.439 \times 10^{+1}$
1202	0.187×10^{-1}	0.142×10^{-1}	0.152×10^{-1}	$0.240 \times 10^{+2}$	**$0.191 \times 10^{+2}$**
1002	0.478×10^{-2}	0.355×10^{-2}	0.687×10^{-2}	**$0.258 \times 10^{+2}$**	$0.435 \times 10^{+2}$
1400	0.161×10^{-2}	0.120×10^{-2}	0.342×10^{-2}	**$0.255 \times 10^{+2}$**	$0.112 \times 10^{+3}$
1200	0.255×10^{-3}	0.148×10^{-3}	0.664×10^{-3}	**$0.421 \times 10^{+2}$**	$0.160 \times 10^{+3}$
1000	0.210×10^{-4}	0.210×10^{-4}	0.210×10^{-4}	0.000×10^{0}	0.000×10^{0}
0408	0.125×10^{-5}	0.110×10^{-5}	0.147×10^{-5}	**$0.119 \times 10^{+2}$**	$0.178 \times 10^{+2}$
0406	0.773×10^{-7}	0.798×10^{-7}	0.303×10^{-7}	**$0.325 \times 10^{+1}$**	$0.608 \times 10^{+2}$
0004	0.435×10^{-7}	0.427×10^{-7}	0.378×10^{-7}	**$0.183 \times 10^{+1}$**	$0.131 \times 10^{+2}$
0206	0.356×10^{-7}	0.350×10^{-7}	0.282×10^{-7}	**$0.162 \times 10^{+1}$**	$0.207 \times 10^{+2}$
0204	0.269×10^{-7}	0.285×10^{-7}	0.230×10^{-7}	**$0.601 \times 10^{+1}$**	$0.147 \times 10^{+2}$
0208	0.211×10^{-7}	0.295×10^{-7}	0.412×10^{-8}	**$0.401 \times 10^{+2}$**	$0.805 \times 10^{+2}$
0404	0.152×10^{-7}	0.134×10^{-7}	0.722×10^{-8}	**$0.122 \times 10^{+2}$**	$0.526 \times 10^{+2}$

TABLE III. Comparison of full CS and statistical CS approximations for the 1006 initial state. Cross sections (Å^2) are shown at E = 100 K for the most efficient transitions in descending order. The left and right % difference columns compare the respective half CS and CS0 results with the full CS approximation. The smaller error is bold-faced in order to show that the half CS approximation performs better than the CS0 approximation in most cases.

Final state	Full CS	Half CS	CS0	% Difference	% Difference
1006	$0.108 \times 10^{+3}$	$0.107 \times 10^{+3}$	$0.113 \times 10^{+3}$	**$0.101 \times 10^{+1}$**	$0.447 \times 10^{+1}$
1204	0.136×10^{-2}	0.114×10^{-2}	0.141×10^{-2}	$0.155 \times 10^{+2}$	**$0.380 \times 10^{+1}$**
1004	0.560×10^{-3}	0.462×10^{-3}	0.925×10^{-3}	**$0.175 \times 10^{+2}$**	$0.650 \times 10^{+2}$
1600	0.321×10^{-3}	0.381×10^{-3}	0.132×10^{-3}	**$0.187 \times 10^{+2}$**	$0.589 \times 10^{+2}$
1404	0.460×10^{-4}	0.438×10^{-4}	0.147×10^{-4}	**$0.485 \times 10^{+1}$**	$0.680 \times 10^{+2}$
1402	0.373×10^{-4}	0.298×10^{-4}	0.454×10^{-4}	**$0.202 \times 10^{+2}$**	$0.217 \times 10^{+2}$
1202	0.116×10^{-4}	0.848×10^{-5}	0.109×10^{-4}	$0.268 \times 10^{+2}$	**$0.594 \times 10^{+1}$**
1002	0.207×10^{-5}	0.140×10^{-5}	0.333×10^{-5}	**$0.322 \times 10^{+2}$**	$0.608 \times 10^{+2}$
1400	0.128×10^{-5}	0.994×10^{-6}	0.263×10^{-5}	**$0.221 \times 10^{+2}$**	$0.106 \times 10^{+3}$
0408	0.175×10^{-6}	0.171×10^{-6}	0.128×10^{-6}	**$0.197 \times 10^{+1}$**	$0.269 \times 10^{+2}$
1200	0.163×10^{-6}	0.969×10^{-7}	0.418×10^{-6}	**$0.404 \times 10^{+2}$**	$0.157 \times 10^{+3}$
0208	0.118×10^{-6}	0.113×10^{-6}	0.151×10^{-6}	**$0.441 \times 10^{+1}$**	$0.278 \times 10^{+2}$
02010	0.103×10^{-6}	0.125×10^{-6}	0.160×10^{-7}	**$0.217 \times 10^{+2}$**	$0.844 \times 10^{+2}$
0006	0.507×10^{-7}	0.510×10^{-7}	0.465×10^{-7}	**0.527×10^{0}**	$0.840 \times 10^{+1}$
0206	0.243×10^{-7}	0.249×10^{-7}	0.271×10^{-7}	**$0.276 \times 10^{+1}$**	$0.117 \times 10^{+2}$

TABLE IV. Comparison of full CS and statistical CS approximations for the 1008 initial state. Cross sections (Å^2) are shown at E = 100 K for the most efficient transitions in descending order. The left and right % difference columns compare the respective half CS and CS0 results with the full CS approximation. The smaller error is bold-faced in order to show that the half CS approximation performs better than the CS0 approximation in most cases.

Final state	Full CS	Half CS	CS0	% Difference	% Difference
1008	$0.110 \times 10^{+3}$	$0.110 \times 10^{+3}$	$0.116 \times 10^{+3}$	**0.793×10^{0}**	$0.459 \times 10^{+1}$
1800	0.598×10^{-3}	0.635×10^{-3}	0.415×10^{-3}	**$0.624 \times 10^{+1}$**	$0.306 \times 10^{+2}$
1206	0.161×10^{-3}	0.142×10^{-3}	0.200×10^{-3}	**$0.117 \times 10^{+2}$**	$0.241 \times 10^{+2}$
1006	0.837×10^{-4}	0.728×10^{-4}	0.146×10^{-3}	**$0.131 \times 10^{+2}$**	$0.739 \times 10^{+2}$
1406	0.977×10^{-5}	0.895×10^{-5}	0.577×10^{-5}	**$0.841 \times 10^{+1}$**	$0.409 \times 10^{+2}$
1404	0.899×10^{-6}	0.768×10^{-6}	0.643×10^{-6}	**$0.145 \times 10^{+2}$**	$0.284 \times 10^{+2}$
1204	0.706×10^{-6}	0.577×10^{-6}	0.859×10^{-6}	**$0.183 \times 10^{+2}$**	$0.217 \times 10^{+2}$
02010	0.514×10^{-6}	0.485×10^{-6}	0.721×10^{-6}	**$0.559 \times 10^{+1}$**	$0.404 \times 10^{+2}$
1604	0.499×10^{-6}	0.482×10^{-6}	0.237×10^{-6}	**$0.352 \times 10^{+1}$**	$0.525 \times 10^{+2}$
04010	0.466×10^{-6}	0.445×10^{-6}	0.473×10^{-6}	$0.452 \times 10^{+1}$	**$0.142 \times 10^{+1}$**
1004	0.177×10^{-6}	0.140×10^{-6}	0.336×10^{-6}	**$0.209 \times 10^{+2}$**	$0.895 \times 10^{+2}$
1600	0.954×10^{-7}	0.839×10^{-7}	0.158×10^{-6}	**$0.121 \times 10^{+2}$**	$0.652 \times 10^{+2}$
1602	0.717×10^{-7}	0.640×10^{-7}	0.761×10^{-7}	$0.108 \times 10^{+2}$	**$0.618 \times 10^{+1}$**
0008	0.625×10^{-7}	0.630×10^{-7}	0.567×10^{-7}	**0.792×10^{0}**	$0.915 \times 10^{+1}$
00010	0.508×10^{-7}	0.461×10^{-7}	0.797×10^{-7}	**$0.923 \times 10^{+1}$**	$0.568 \times 10^{+2}$

upon if an appropriate functional form was developed that takes advantage of this smooth dependence.

IV. CONCLUSIONS

The accuracy of the CS approximation for H_2+H_2 collisions was studied for translational energies less than 100 K by comparison with results obtained using the numerically exact CC formulation. Both sets of calculations were performed on a state-of-the-art PES[16] which allows for full-dimensional dynamics. The CS approximation was found to give quantitative accuracy for elastic scattering and for pure vibrational and rotational transitions involving only one molecule. It was also found to be generally reliable for estimating relative cross sections. Exceptions were observed when both molecules undergo multi-quantum changes. Transitions involving multi-quantum changes are often inefficient which would reduce the significance of the discrepancies in such cases.

An extensive study of the Ω-dependency of the CS cross sections was performed in order to find ways to further reduce the computational cost of the calculations and to provide insight into the internal energy transfer mechanisms. The variability in the partial cross sections for different values of Ω was found to be too large to apply the statistical approximation introduced previously.[26] A modified statistical CS approximation was introduced which calculates partial cross sections for only non-negative even projections and cuts the computational time in half compared to the full CS approximation. The results were found to be reliable to within 20% for transitions with $\min[\Omega_{max}, \Omega'_{max}] \geq 4$ and tended to improve as Ω_{max} increases. The computational efficiency also improves with Ω due to the decreasing number of j_{12} values which must be included in the basis set. Therefore, the CS approximation offers a practical means to compute cross sections for diatom-diatom systems which have significant rotational excitation.

Although no results are presented for ortho-ortho collisions, preliminary calculations have found that the exchange-permutation symmetrized cross sections $\sigma^{\varepsilon_P=\pm 1}$ are virtually identical for collision energies above 20 K. This observation suggests that a single exchange symmetry may be used, similar to the para-para case, which would provide an additional computational cost saving. For ortho-para collisions, the full distinguishable basis sets are considerably larger than the exchange symmetrized basis sets, and the computational cost of the CC method is very high even for low-lying initial states.[22] The CS approximation is likely to be the best option for this case and may be expected to provide comparable accuracy to the para-para cross sections presented here.

The results of this work are encouraging for other diatom-diatom systems which have more closely spaced rotational levels. An important example is H_2+CO in low density astrophysical environments which typically require a non-LTE analysis for excited rotational levels. Previous calculations for this system[36] have already demonstrated good agreement between CS and CC formulations when using the rigid rotor approximation. It would be desirable to extend these calculations to include a full-dimensional treatment. As in the present case, a combination of CC and CS methods would likely be needed to obtain a large set of state-to-state rate coefficients for use in the astrophysical models.

ACKNOWLEDGMENTS

The work of A.B., S.P., and R.C.F. was supported by NSF Grant No. PHY-1203228. N.B. acknowledges support from NSF Grant No. PHY-1205838, and P.C.S. acknowledges support from NASA Grant No. NNX12AF42G.

[1] *Molecular Hydrogen in Space*, edited by F. Combes and G. Pineau des Forets (Cambridge University Press, 2000).
[2] S. C. O. Glover and T. Abel, MNRAS **388**, 1627 (2008).
[3] B. T. Draine and F. Bertoldi, Astrophys. J. **468**, 269 (1996).

[4]D. J. Hollenbach and A. G. G. M. Tielens, Rev. Mod. Phys. **71**, 173 (1999).
[5]G. Shaw, G. J. Ferland, N. P. Abel, P. C. Stancil, and P. A. M. van Hoof, Astrophys. J. **624**, 794 (2005).
[6]M.-M. Audibert, R. Vilaseca, J. Lukasik, and J. Ducuing, Chem. Phys. Lett. **31**, 232 (1975).
[7]W. Meier, G. Ahlers, and H. Zacharias, J. Chem. Phys. **85**, 2599 (1986).
[8]T. G. Kreutz, J. Gelfand, R. B. Miles, and H. Rabitz, Chem. Phys. **124**, 359 (1988).
[9]R. L. Farrow and D. W. Chandler, J. Chem. Phys. **89**, 1994 (1988).
[10]B. Maté, F. Thibault, G. Tejeda, J. M. Fernández, and S. Montero, J. Chem. Phys. **122**, 064313 (2005).
[11]T. Ahn, I. Adamovich, and W. R. Lempert, Chem. Phys. **335**, 55 (2007).
[12]S. Green, J. Chem. Phys. **62**, 2271 (1975).
[13]D. W. Schwenke, J. Chem. Phys. **89**, 2076 (1988).
[14]A. Aguado, C. Suárez, and M. Paniagua, J. Chem. Phys. **101**, 4004 (1994).
[15]A. I. Boothroyd, P. G. Martin, W. J. Keogh, and M. J. Peterson, J. Chem. Phys. **116**, 666 (2002).
[16]R. J. Hinde, J. Chem. Phys. **128**, 154308 (2008).
[17]D. R. Flower and E. Roueff, J. Phys. B **31**, 2935 (1998).
[18]D. R. Flower and E. Roueff, J. Phys. B **32**, 3399 (1999).
[19]G. Quéméner, N. Balakrishnan, and R. V. Krems, Phys. Rev. A **77**, 030704(R) (2008).
[20]G. Quéméner and N. Balakrishnan, J. Chem. Phys. **130**, 114303 (2009).
[21]N. Balakrishnan, G. Quéméner, R. C. Forrey, R. J. Hinde, and P. C. Stancil, J. Chem. Phys. **134**, 014301 (2011).
[22]S. Fonseca dos Santos, N. Balakrishnan, S. Lepp, G. Quemener, R. C. Forrey, R. J. Hinde, and P. C. Stancil, J. Chem. Phys. **134**, 214303 (2011).
[23]B. Yang, R. C. Forrey, P. C. Stancil, S. Fonseca dos Santos, and N. Balakrishnan, Phys. Rev. Lett. **109**, 233201 (2012).
[24]S. Fonseca dos Santos, N. Balakrishnan, R. C. Forrey, and P. C. Stancil, J. Chem. Phys. **138**, 104302 (2013).
[25]M. H. Alexander and A. E. DePristo, J. Chem. Phys. **66**, 2166 (1977).
[26]T. G. Heil, S. Green, and D. J. Kouri, J. Chem. Phys. **68**, 2562 (1978).
[27]S. K. Pogrebnya and D. C. Clary, Chem. Phys. Lett. **363**, 523 (2002).
[28]S. Y. Lin and H. Guo, J. Chem. Phys. **117**, 5183 (2002).
[29]S. K. Pogrebnya, M. E. Mandy, and D. C. Clary, Int. J. Mass Spectrom. **223–224**, 335 (2003).
[30]S. Y. Lin and H. Guo, Chem. Phys. **289**, 191 (2003).
[31]R. V. Krems, *TwoBC – quantum scattering program* (University of British Columbia, Vancouver, Canada, 2006).
[32]B. R. Johnson, J. Comput. Phys. **13**, 445 (1973).
[33]D. E. Manolopoulos, J. Chem. Phys. **85**, 6425 (1986).
[34]B. Yang, H. Perera, N. Balakrishnan, R. C. Forrey, and P. C. Stancil, J. Phys. B **39**, S1229 (2006).
[35]R. C. Forrey, Phys. Rev. A **66**, 023411 (2002).
[36]B. Yang, P. C. Stancil, N. Balakrishnan, and R. C. Forrey, Astrophys. J. **718**, 1062 (2010).